

# Tides of the Eastern Bering Sea Shelf



Carl A. Pearson,<sup>1</sup> Harold O. Mofjeld,<sup>2</sup> and Richard B. Tripp<sup>3</sup>

<sup>1</sup> National Ocean Survey, assigned to:  
Pacific Marine Environmental Laboratory/NOAA  
Seattle, Washington

<sup>2</sup> Pacific Marine Environmental Laboratory/NOAA  
Seattle, Washington

<sup>3</sup> Department of Oceanography  
University of Washington  
Seattle, Washington

## ABSTRACT

The acquisition of a substantial amount of pressure-gauge and current-meter data on the Bering Sea shelf has permitted a much more accurate description of the tides than has previously been possible. Cotidal charts are presented for the  $M_2$  and, for the first time, the  $N_2$ ,  $K_1$ , and  $O_1$  constituents, and tidal current ellipse charts for  $M_2$  and  $K_1$ .  $S_2$ , normally the second largest semidiurnal constituent, has not been included because it is anomalously small in the Bering Sea. The tide enters the Bering Sea through the central and western Aleutian Island passes and progresses as a free wave to the shelf. Largest tidal amplitudes are found over the southeastern shelf region, especially along the Alaska Peninsula and interior Bristol Bay. Each semidiurnal tide propagates as a Kelvin wave along the Alaska Peninsula but appears to be converted on reflection in interior Bristol Bay to a Sverdrup wave. A standing Sverdrup (Poincaré) wave resulting from cooscillation in Kuskokwim Bay is evident on the outer shelf. The semidiurnal tides are small in Norton Sound where there is an amphidrome. The diurnal tides, which can have only Kelvin wave dynamics, cooscillate between the deep basin and the shelf. Amphidromes are found between Nunivak Island and the Pribilof Islands, and west of Norton Sound. Throughout most of the shelf the tide is of the mixed, predominantly semidiurnal type; however, the diurnal tide dominates in Norton Sound.

Tidal models by Sünderman (1977) (a vertically integrated  $M_2$  model of the entire Bering Sea) and by Liu and Leendertse (1978, 1979) (a three-dimensional model of the southeastern shelf incorporating the diurnal and semidiurnal tides) are discussed. Good qualitative agreement is found between the models and observations.

## INTRODUCTION

As with most continental shelves, the tides and tidal currents on the eastern Bering Sea shelf play important roles in such oceanographic processes as the maintenance of the density structure, sediment resuspension and transport, and the distributions of benthic and intertidal organisms. A knowledge of the tides and tidal currents is therefore necessary in order to understand the region's oceanography. The tides of the Bering Sea have been of interest to physical oceanographers and astronomers for a long time (e.g., Jeffreys 1921, Munk and MacDonald 1960, Cartwright 1979). This interest has been based on the premise that the vast continental shelves of the Bering Sea (Fig. 8-1), with their proximity to the Pacific Ocean, act as a major sink of the world's tidal energy. Yet many aspects of the tides and tidal currents in the Bering Sea have remained unknown because inadequate data made it impossible to draw definitive cotidal charts or to obtain reliable boundary conditions for numerical models. Fortunately, in recent years a large number of pressure-gauge and current-meter observations have been made on the eastern Bering Sea continental shelf, and the new data make possible a more detailed description of the tides in the eastern Bering Sea.

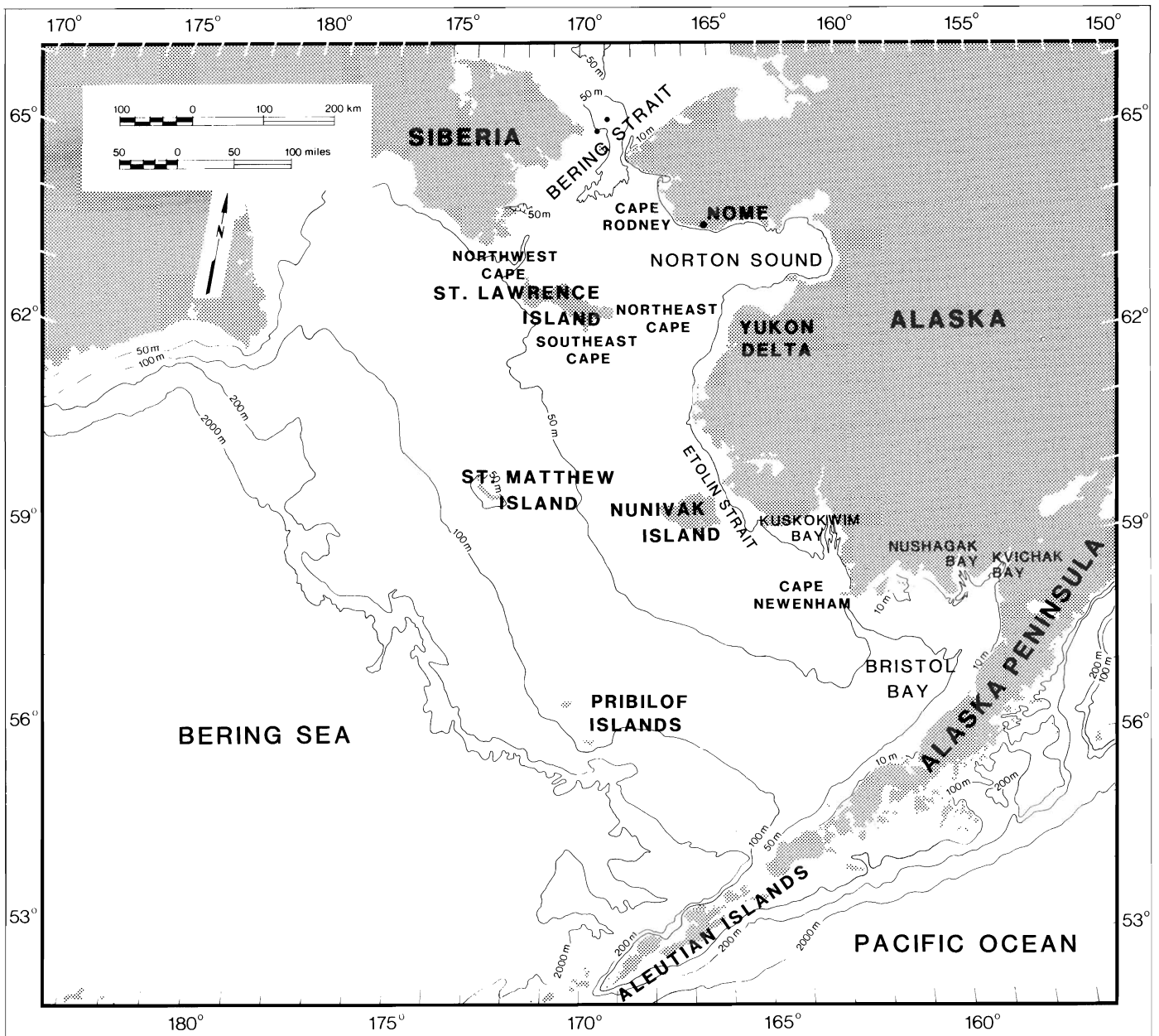


Figure 8-1. Bathymetric chart of the Bering Sea.

Concurrent with the recent field work has been the development of several numerical models for tides in part or all of the Bering Sea. One of these, the Liu and Leendertse (1978, 1979) model of Bristol Bay, will be described in detail. The other models are discussed briefly for completeness and to show the reader the scope of current theoretical work. The field work is also continuing. In a sense then, this chapter is a progress report as well as a review of past work and a description of new results.

The tides that we shall be concerned with are the principal tidal constituents  $N_2$  and  $M_2$  in the semi-

diurnal band (periods of about 0.5 days) and  $O_1$  and  $K_1$  in the diurnal band (periods of about 1.0 day). Ordinarily, the principal solar semidiurnal constituent  $S_2$  would be included in the discussion. However,  $S_2$  is anomalously small throughout the Bering Sea, possibly because it has small amplitudes in the adjacent North Pacific Ocean. Whatever the reason, no consistent distribution for  $S_2$  appears in the field data above the background noise level. The complicated distributions of semidiurnal and diurnal tides in the Bering Sea produce a rich variety of tidal types, ranging from fully semidiurnal in some regions to

fully diurnal in others. Sample time series will be shown later in the chapter to illustrate the tidal types. Probably the most important figures are the cotidal charts for the four principal constituents, because from these charts it is possible to infer much about the dynamics of the tides and to obtain harmonic constants for tidal predictions. Empirical cotidal charts derived from recent data and theoretical cotidal charts from models will be presented.

The discussion of tidal currents in the Bering Sea will be presented with less certainty than that of the tides, because the few early measurements of tidal currents were of short duration and mostly limited to harbors and nearshore regions, and the recent observations from offshore current meters occasionally suffered from errors due to biological fouling and effects of wave motion. Still, with careful study and editing of the recent data reasonably accurate tidal current harmonic constants can be obtained for most areas. These results help define the dynamics controlling the tidal motion.

The setting for the tidal and tidal current distributions can be obtained from previous work (Harris 1904, Leonov 1960, Office of Climatology and Oceanographic Analysis Division 1961, Defant 1961, Coachman et al. 1975) which for the most part describes the semidiurnal tide. The tide wave enters the Bering Sea as a progressive wave from the North Pacific Ocean, mainly through the central and western passages of the Aleutian-Komandorski Islands. The Arctic Ocean is a minor secondary source of tides which propagate southward into the north Bering Sea where they complicate the tidal distributions. The North Pacific and Arctic Oceans are also sinks of tidal energy for tides propagating out of the Bering Sea. Tides in the Bering Sea are considered to be the result of cooscillation with large oceans. Once inside the Bering Sea, each tidal constituent propagates as a free wave subject to the Coriolis effect and bottom friction.

The tide wave propagates rapidly across the deep western basin. Part of it then propagates onto the southeast Bering shelf where large amplitudes are found along the Alaska Peninsula and in Kvichak and Kuskokwim Bays. Another part propagates northeastward past St. Lawrence Island and into Norton Sound. Over most of the shelf region the tide is mainly semidiurnal, but in Norton Sound the diurnal tides predominate. A number of amphidromic systems are formed on the eastern Bering shelf and in Norton Sound as a result of the interference of tides propagating from various directions. Various authors have different opinions about the details of the tidal height and current distributions, including the exist-

ence, shape, and location of amphidromic systems. Some of the controversy can be resolved with the recently acquired data; the rest will require more observations and/or complete models.

## NUMERICAL MODELS

Several numerical models have been applied to the tides in the Bering Sea. They are of two basic types: vertically integrated models which simulate horizontal distributions and three-dimensional models which simulate vertical variations as well. Some of these models are still under development.

The vertically integrated models by Hastings (1976) and Sünderman (1977) superimpose uniformly spaced grids over the Bering Sea Shelf and the entire Bering Sea, respectively. Finite difference approximations to the dynamic equations with quadratic bottom friction are solved over the grids as initial value problems in time with lateral friction included to stabilize the calculation. The tides enter the models as boundary conditions along the open boundaries; time series of sea level at the open boundaries drive the motion in the interior with zero flux and no-slip conditions imposed along coasts. The imposed time series are derived from harmonic constants interpolated from observed values at islands and on coasts. After integrating the models through an initial transient, the motion can be analyzed for tides and tidal currents. Since Hastings (1976) does not take this step, we show only results of the model by Sünderman (1977), which is limited to the  $M_2$  semidiurnal constituent (Fig. 8-2) and its consequences in time-averaged properties and higher harmonics.

A distinctly different, vertically integrated model is under development by Preisendorfer (1979), who uses Bristol Bay to illustrate a new technique. The technique involves computing the linear response of a region to a long wave of a given frequency, such as a tidal constituent, as a synthesis of responses to simple subregions. Since realistic boundary conditions were not used in the Bristol Bay example, the results of the calculation may be considered preliminary. Further work on the technique is planned (Preisendorfer, personal communication).

A three-dimensional model has been developed by Leendertse and Liu (1977) and Liu and Leendertse (1978, 1979) to predict tides and wind-driven currents on the southeast Bering shelf for the prediction of oil spill trajectories and for risk analysis. The grid for the model (Fig. 8-3a) is uniform in the horizontal dimensions but packed in the vertical dimension to allow higher resolution of the pycno-

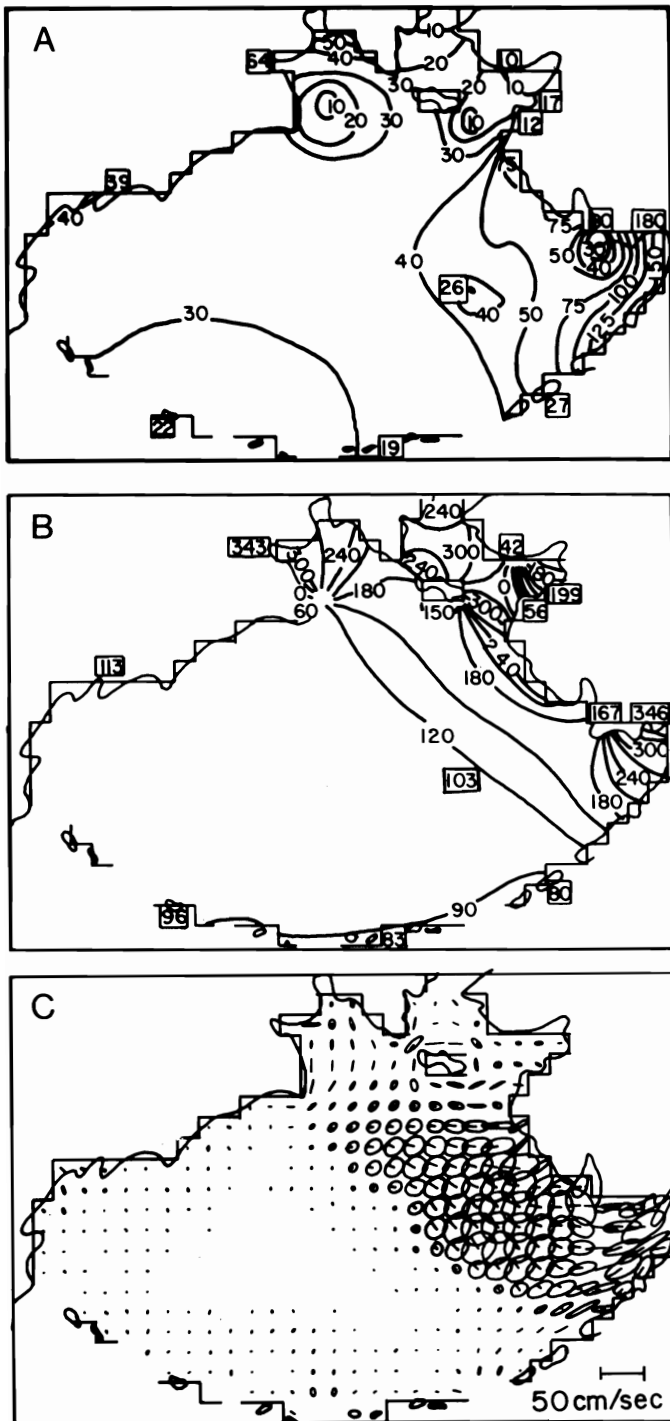


Figure 8-2. Charts of (a) coamplitude (cm), (b) cophase (Greenwich lag in degrees), and (c) tidal current ellipses (cm/sec; radial line within each ellipse represents the tidal velocity at Greenwich transit) from the vertically integrated model by Sünderman (1977) of the  $M_2$  tide in the Bering Sea. For the finite-difference model: the grid size is 75 km; the time step is 223.5 sec; the bottom drag coefficient is 0.003; and the lateral viscosity is  $10^9$   $\text{cm}^2/\text{sec}$ . The numbers appearing in boxes are observed values. (Reproduced with permission from J. Sünderman, 1977, *Deutsche Hydrographische Zeitschrift*, 91-101, Figs. 3, 4, 5).

cline. The dynamic variables are the horizontal and vertical velocity components, temperature, salinity, density, pressure, and the energy density at sub-grid scales; a passive contaminant can also be included in the model. The large-scale (resolved by the grid) variables satisfy a relatively complete set of nonlinear dynamic equations averaged over each vertical layer and specialized to the extent that the hydrostatic equation is used in the vertical direction. The subgrid scale turbulence satisfies a one-equation closure model in the turbulent energy density.

Within the dynamic equations are viscous and diffusive terms. The associated viscosities and diffusivities in the horizontal direction have contributions from the large-scale motions through the local vorticity gradient. The contributions of the subgrid turbulence for each direction depend upon a turbulent Richardson number which includes the local density gradient and the local subgrid energy density. The formulas for the turbulent contributions are modified from Mamayev (1958) and include empirical coefficients chosen to produce reasonable behavior of the turbulence in the presence of stratification. Liu (personal communication) indicates that newer versions of the model under development will use a different formulation for the turbulent viscosities and diffusivities which eliminates many of the empirical coefficients.

The motion in the lowest layer is subject to bottom boundary conditions. The bottom is assumed to be impervious and insulating so that zero flux of heat, salt, and water occurs through the bottom. The bottom boundary condition for momentum is a quadratic friction law in which the Chezy coefficient is adjusted to match model currents with observed currents. At the free surface, a uniform wind stress can be imposed over the region to produce wind-driven currents in addition to the tidal motion. The model is integrated as an initial value problem with predicted tide-level time series specified along the open boundaries; these time series are obtained through interpolation of harmonic constants derived from bottom pressure data.

To simulate tides and tidal currents on the southeast Bering shelf, Liu and Leendertse (1978, 1979) chose a period, 16-18 June 1976, for which extensive observations existed, some collected specifically in support of this modelling effort. The model was run for a total of 63 hours, which included an initial transient preceding the comparison period. Time series of sea level were then Fourier analyzed for composite semidaily and daily tides from which cotidal charts (Fig. 8-4a,b) were constructed. A more

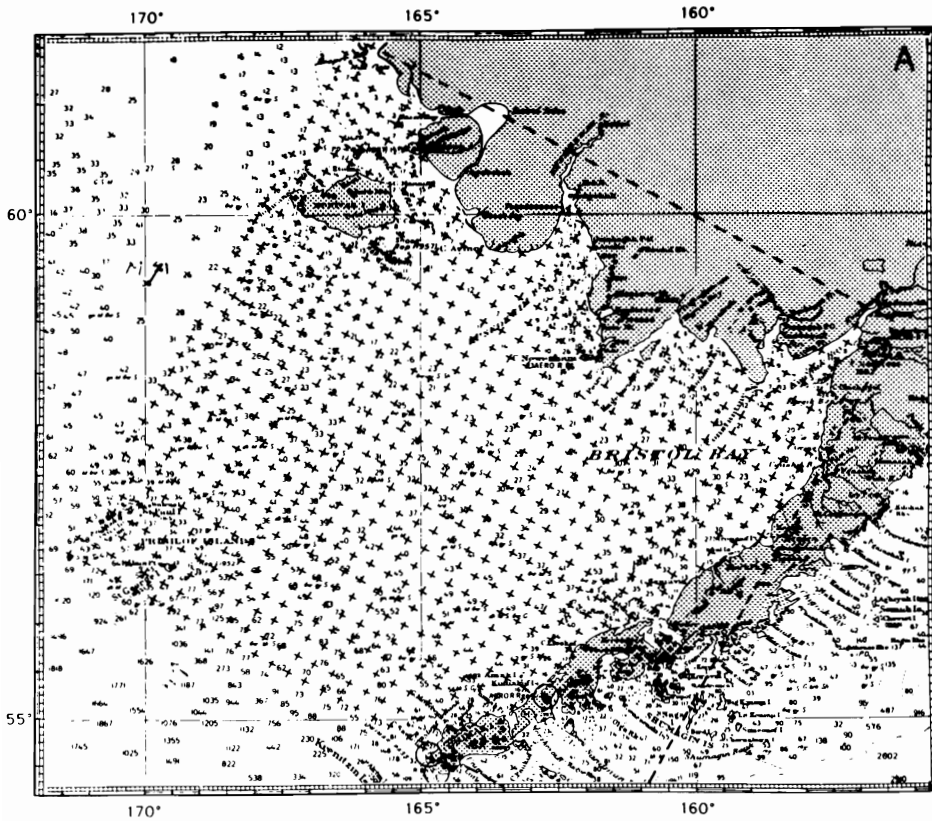
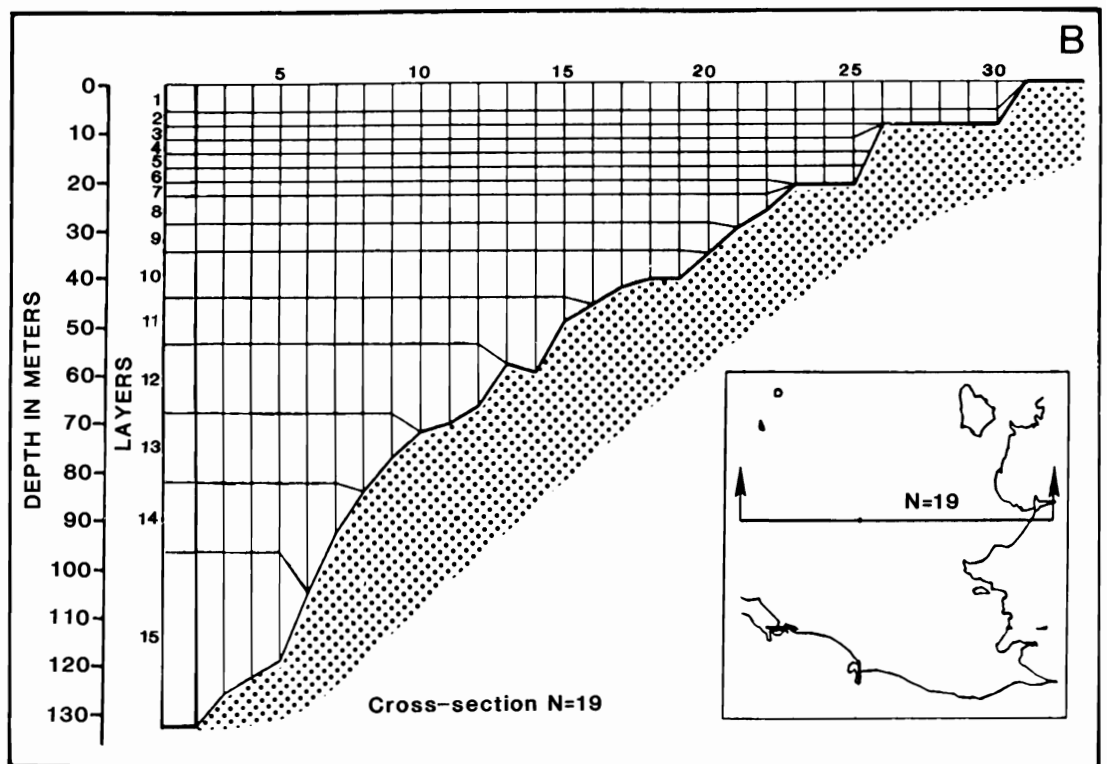


Figure 8-3a, b. (a) The horizontal grid and (b) a section showing the vertical grid of the three-dimensional, turbulent energy model of the south-eastern Bering Shelf by Liu and Leendertse (1978, 1979). The horizontal grid spacing is 21.82 km; the vertical spacing in this 14-layer model is variable to allow high resolution in the pycnocline. The time step for the model is 180 sec, and the Chezy coefficient of bottom drag is 700 ( $\text{cm}^{1/2}/\text{sec}$ ). (Reproduced with permission from S. K. Liu and J. J. Leendertse 1979).



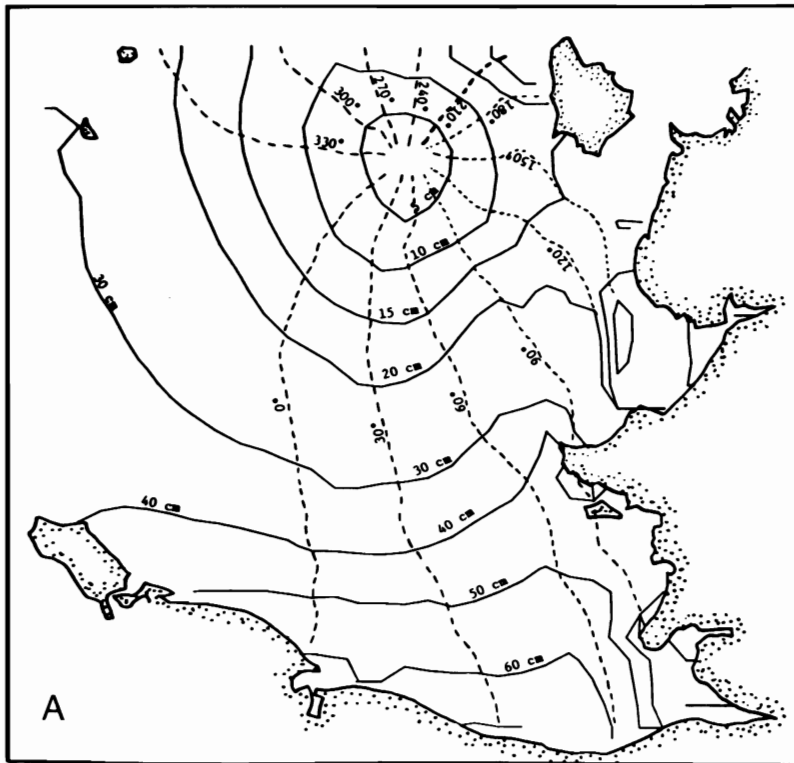
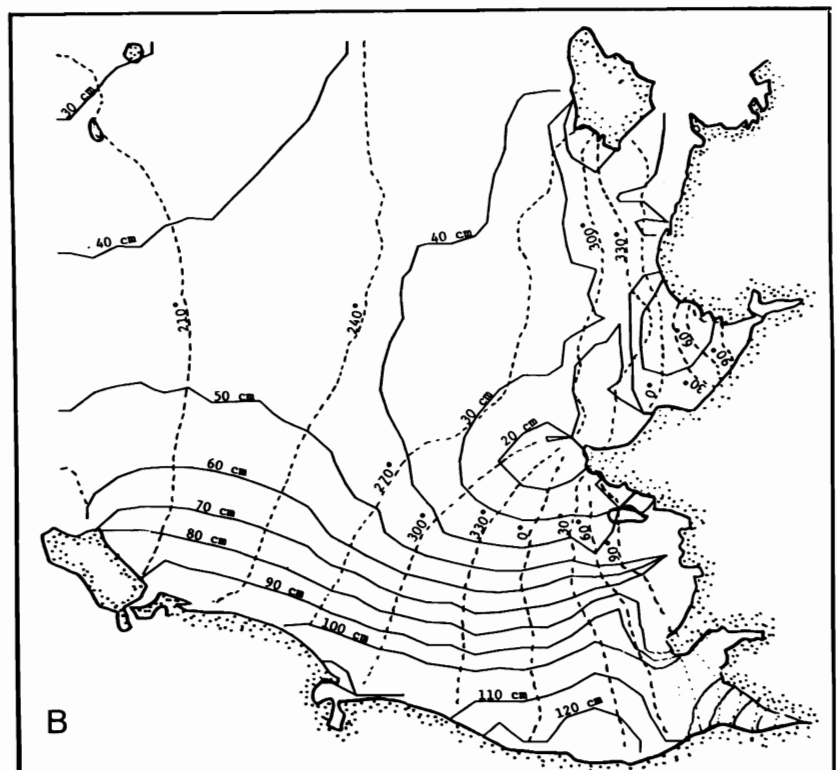


Figure 8-4a, b. Theoretical cotidal charts (amplitudes in cm, phases in degrees relative to the start of the simulation) for (a) the composite diurnal tide and (b) the composite semidiurnal tide obtained from the three-dimensional, turbulent energy model by Liu and Leendertse (1978) of the southeastern Bering shelf. (Reproduced with permission from S K. Liu and J. J. Leendertse 1979.)



detailed analysis into individual tidal constituents was not possible because of the short series length. After model coefficients were adjusted to match current data, a set of time series (Fig. 8-5a-c) of currents and water properties was produced.

A similar three-dimensional model is under development for Norton Sound (Liu, personal communication). It includes improved equations for the subgrid-scale turbulence. The model can also impose sea ice on the water; ice in the north Bering Shelf region can be expected to modify the tidal and wind-driven responses significantly.

## OBSERVATIONS

Offshore pressure and current observations, made on the east Bering Shelf (Fig. 8-6) during 1975-78, are a major new source of information about tidal heights and currents. These data have been analyzed<sup>1</sup> for harmonic constants and tidal current ellipses; the analysis will be presented in this section. To these results have been added historical harmonic constants from the International Hydrographic Bureau (1966) and results of analysis of previously unpublished data from the National Ocean Survey and the U.S. Geological Survey.

### *Tidal observations*

Empirical cotidal charts (Figs. 8-7 through 8-10) have been constructed for the four largest tidal constituents:  $M_2$ ,  $N_2$ ,  $K_1$ , and  $O_1$ . These charts were constructed as follows: Cotidal lines were drawn by interpolation where the station spacing is relatively small compared with the spatial scales of a given tidal constituent. Elsewhere, the positions of cotidal lines were estimated either by shifting the distribution of lines from numerical models to match observed values, or by estimation with reference to hydrodynamic considerations. Like all empirical cotidal charts, these charts are somewhat subjective. On each of the cotidal charts, regions of particular uncertainty are denoted by question marks.

An example of the procedure for drawing charts can be seen from the portion of the  $M_2$  chart (Fig. 8-7) around St. Lawrence Island. Along the northern shore of the island,  $M_2$  harmonic constants can be found for enough stations to document the westward progression of phase without reference to models. Along the southern shore of the island there are fewer

stations, and the convergence of  $M_2$  cophase lines at Southeast Cape was drawn with reference (Fig. 8-2) to the  $M_2$  model by Sündermann (1977). The records along the northern coast of St. Lawrence Island provide harmonic constants for  $M_2$  derived from a high water/low water analysis (see Appendix). These data are not sufficient to allow a determination of harmonic constants of other constituents; the cotidal charts of those constituents in this region are therefore more speculative than that of  $M_2$ .

The cotidal charts show the complex distribution of tidal amplitudes and phases over the eastern shelf region. Largest amplitudes for all constituents are found along the Alaska Peninsula, interior Bristol Bay, and in Kuskokwim Bay. The smallest tides are found on the outer shelf and north of St. Lawrence Island. A number of amphidromes are present; there is a semidiurnal amphidrome in Norton Sound and a virtual amphidrome at Cape Newenham, while diurnal amphidromes are found on the southeast shelf between Nunivak Island and the Pribilof Islands and west of Norton Sound. The last is evident only for the  $K_1$  constituent. The situation is more ambiguous for the  $O_1$  tide north of St. Lawrence Island, possibly because the longer wavelength of  $O_1$  would place an amphidrome farther west of the offshore stations. The phase difference between  $K_1$  and  $O_1$  changes rapidly at stations in this area, indicating that the structures of the two constituents are significantly different.

The  $S_2$  tide, normally the second largest semidiurnal constituent, is unusually small throughout the Bering Sea. Typically,  $S_2$  amplitudes range from 1 to 3 cm. The cotidal charts by Bogdanov (1961) and Bogdanov et. al. (1964) for the North Pacific Ocean show an  $S_2$  amphidrome just south of the Aleutian Islands. Perhaps the small  $S_2$  amplitude where tides propagate into the Bering Sea produces small  $S_2$  amplitudes throughout the region. Since analysis of data from the Bering Sea did not produce stable  $S_2$  harmonic constants, a cotidal chart for  $S_2$  could not be constructed. A result of the small  $S_2$  is that the fortnightly inequality, or semidiurnal spring-neap cycle, is much less important than the parallactic inequality due to the variation in the moon's distance from the earth. This cycle is equal to the period of the moon's orbit, 27.55 days, and is manifested in the beat of  $N_2$  against  $M_2$ .

Tidal type may be classified (e.g., Defant 1961) by the value of the ratios of the sums of amplitudes of principal diurnal constituents  $K_1$  and  $O_1$  the principal semidiurnal constituents  $M_2$  and  $S_2$ .

<sup>1</sup> Details of the analysis procedure and results are given in the Appendix.

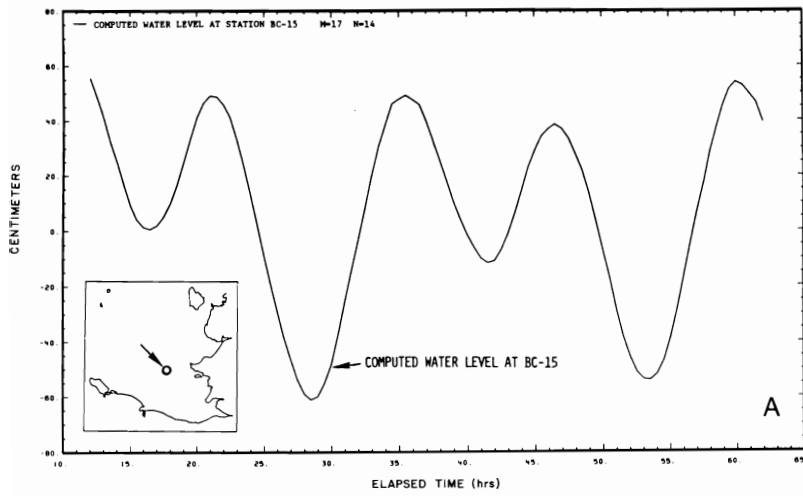
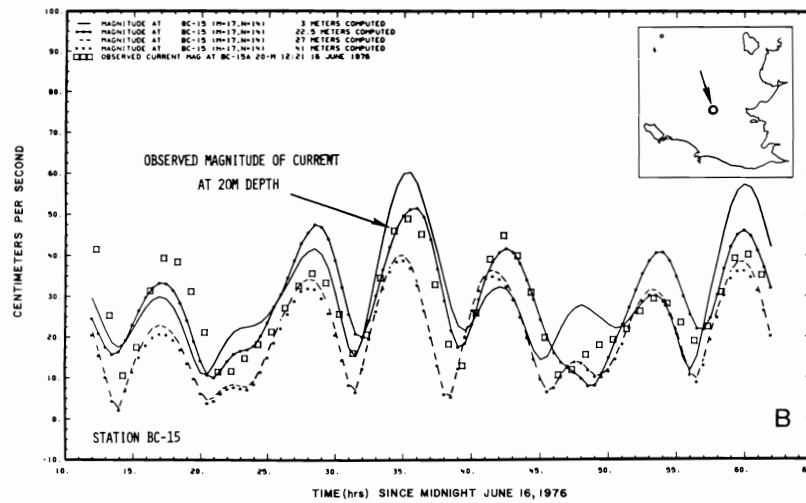
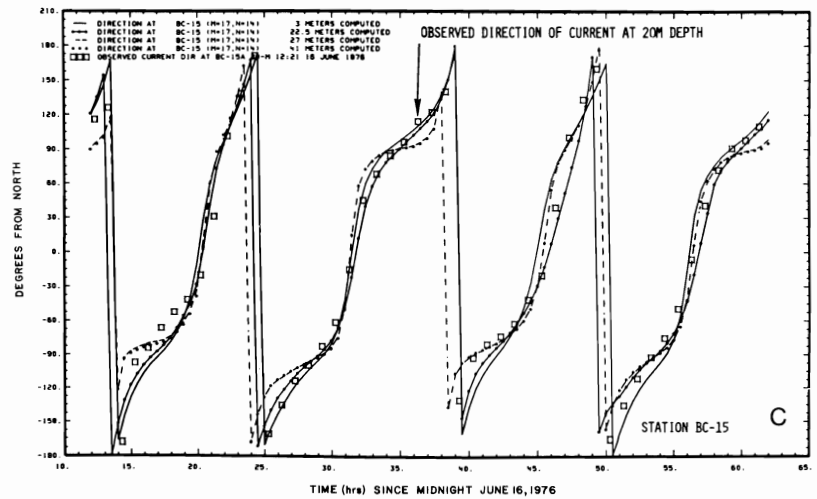


Figure 8-5a-c. Time series at Station BC-15 ( $57^{\circ}36'N$ ,  $162^{\circ}45'W$ ) from the three-dimensional, turbulent energy model by Liu and Leendertse (1978) for (a) sea-level displacement, (b) current speed, and (c) current direction during the period 0000 GMT 16 June 1976 through 1400 GMT 18 June 1976. (Reproduced with permission from S. K. Liu and J. J. Leendertse 1979.)



TIME (hrs) SINCE MIDNIGHT JUNE 16, 1976



TIME (hrs) SINCE MIDNIGHT JUNE 16, 1976

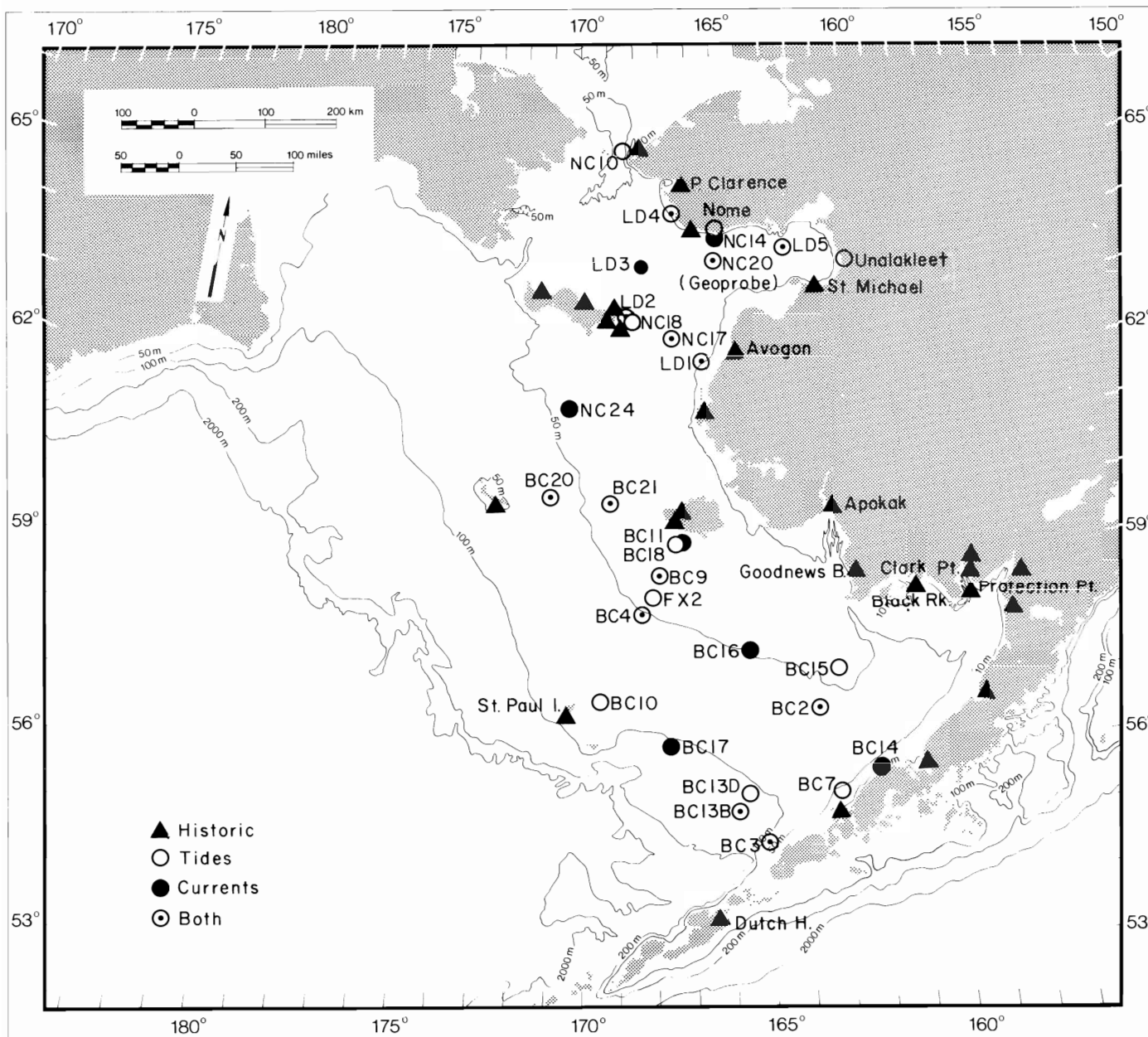


Figure 8-6. Location of stations used in construction of cotidal and tidal current ellipse charts. Historic stations with names had harmonic constants available; those without names were used to estimate  $M_2$  from high and low water analysis.

Since  $S_2$  is so small in the Bering Sea we have substituted  $N_2$  in the equation:

$$F = \frac{K_1 + O_1}{M_2 + N_2}$$

Values of  $F$  less than 0.25 denote regular semidiurnal tides, with two high and two low waters per day of approximately the same height. The mixed, predominantly semidiurnal type has values of 0.25-1.5 and is characterized by two high and two low waters per day, but with large diurnal inequalities in heights. Mixed predominantly diurnal tides,  $F = 1.5-3.0$ , have only one high and one low water per day when the

moon is near its maximum declination. Regular diurnal tides have values of  $F$  greater than 3.0 and usually have only one high and one low water per day.

In most areas of the eastern Bering Sea the tide is the mixed semidiurnal type. The regular semidiurnal type is found in the Bering Strait and in a small area near the diurnal amphidrome south of Nunivak Island. The mixed diurnal type is found along the Aleutian chain, probably near Cape Newenham and in eastern Norton Sound. Regular diurnal tides are found in the vicinity of the semidiurnal amphidrome in Norton Sound.

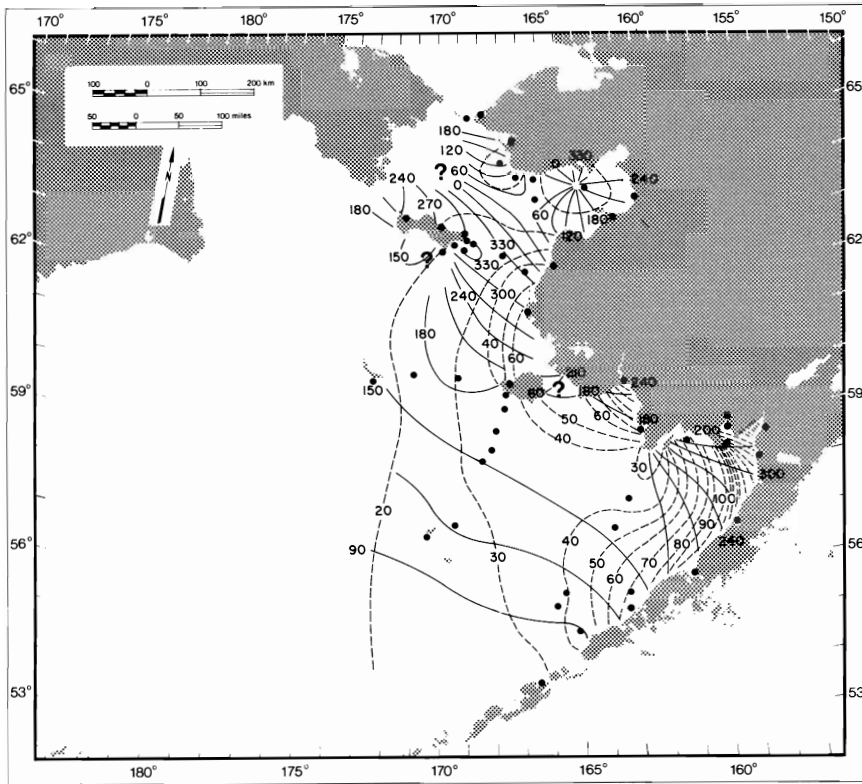


Figure 8-7.  $M_2$  cotidal chart based on the new observations. Dots represent locations of stations used in construction of the chart. Solid lines are cophase lines referred to Greenwich. Dashed lines are coamplitude, in centimeters. Areas of major uncertainty are denoted by question marks.

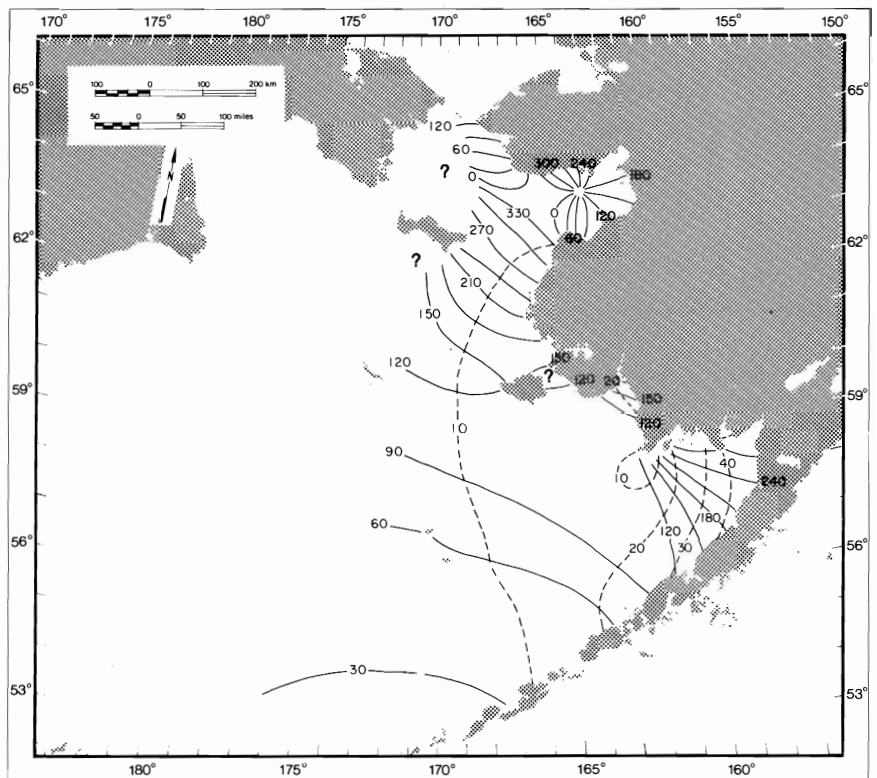


Figure 8-8. Same as 8-7 but for  $N_2$ .

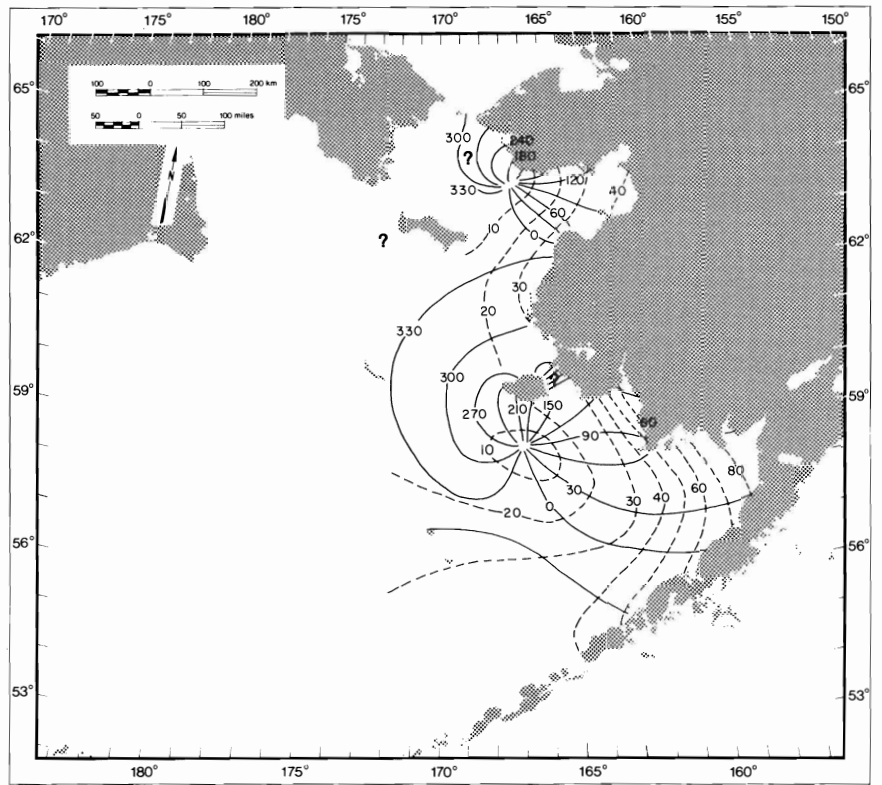


Figure 8-9. Same as 8-7 but for  $K_1$ .

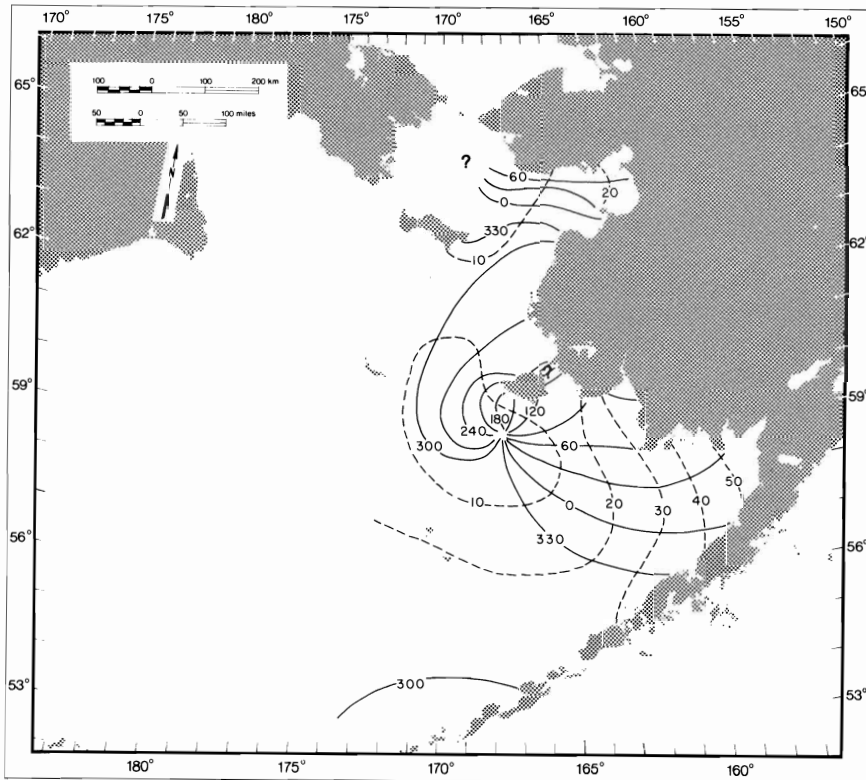


Figure 8-10. Same as 8-7 but for  $O_1$ .

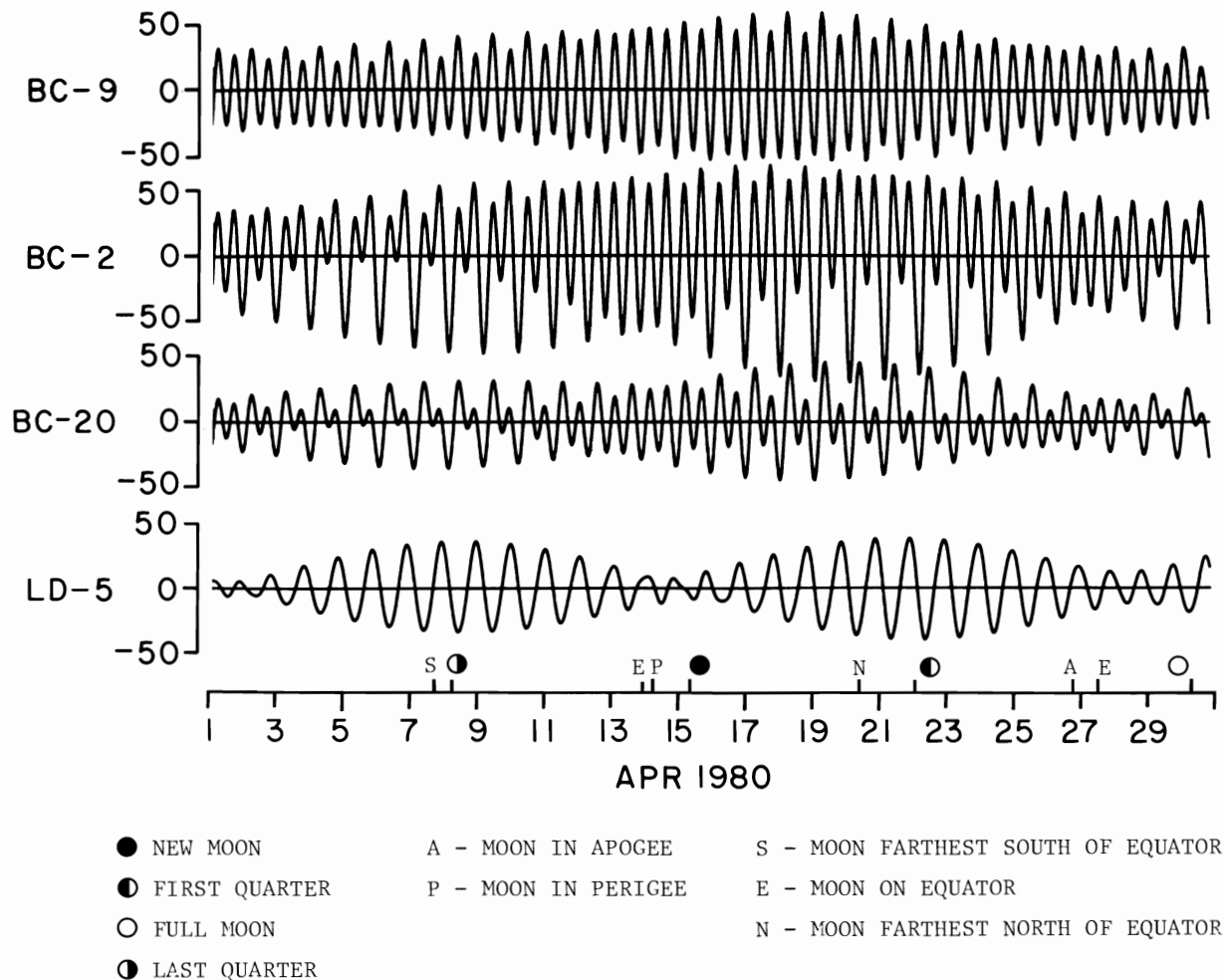


Figure 8-11. Predicted tides for the month of April 1980 for selected stations, illustrating tidal types found in the Bering Sea. Predictions used  $M_2$ ,  $N_2$ ,  $S_2$ ,  $K_1$ ,  $O_1$ , and  $P_1$ .

Examples of different tide types are shown in Fig. 8-11, which shows predicted tide curves for the month of April 1980. Station BC9, southwest of Nunivak Island near the diurnal amphidrome, has an  $F$ -value of 0.25 and is mainly semidiurnal. The lunar perigee is on the 14th with the largest range on about April 18 and the smallest at the beginning and end of the month. BC2 in Bristol Bay has the mixed semidiurnal type with  $F = 0.79$ . The inequalities are largest after maximum declination of the moon on the 7th and 20th. BC20, near St. Matthew Island, also has a mixed semidiurnal tide,  $F = 1.02$ . Note that while at BC2 the diurnal inequality is mainly in the low tide, at BC20 it is in both the high and low waters. This is caused by differences in the phase relationships between the major diurnal ( $O_1 + K_1$ ) tides and  $M_2$ . Finally, the regular diurnal tide type is found at LD5, near the semidiurnal amphidrome in

Norton Sound. Here  $F = 16.3$  and the fortnightly tropic-equatorial tide cycle, caused by the declination of the moon, is evident.

#### *Tidal current observations*

Harmonic constants of current-meter data are subject to more variability in time and space than those of pressure-gauge data, which are generally quite stable. A variety of factors affect observed tidal current velocities, including local bathymetry and depth, shear in the water column, and increased damping and friction in the upper layers due to ice cover. In addition, the Savonius rotor current meters used in this study were occasionally subject to errors due to wave-induced mooring motion, which resulted in higher recorded speeds, and biological fouling of the rotor by algae and various types of drifting

marine organisms, resulting in lower recorded speeds.

To examine temporal variability, successive 29-day harmonic tide analyses were performed on all available current-meter data. Analyses were performed on the east and north components of velocity. Several moorings had decreases in tidal amplitudes corresponding to times of ice cover. Generally, the semidiurnal constituents were reduced more than the diurnal constituents, and reductions were greatest for the upper meters. Phases were also affected. Fig. 8-12 shows variations in the  $M_2$  constituents of the east component of current at station NC24 at depths of 24 m and 40 m for a one-year period beginning 19 September 1977 (the north component exhibited similar behavior). Ice began forming in the area of the mooring in late November and early December of 1977 (Fleet Weather Facility 1977 and 1978); this ice formation was associated with a decrease in the  $M_2$  amplitude at the upper meter to 18 cm/sec. However, the amount of ice over the mooring and the location of the ice edge varied until February 1978, when the ice edge moved much further south. Amplitudes were lowest in February and March during the time of extensive ice cover and then increased again as the ice broke up. Amplitudes were reduced by almost 40 percent, from 22 cm/sec in the early fall to about 14 cm/sec during late winter. During the summer 1978 amplitudes returned to over 20 cm/sec. The effect was much less at the lower meter. Amplitudes were decreased from 15.4 cm/sec to about 12.5 cm/sec or less than 20 percent.

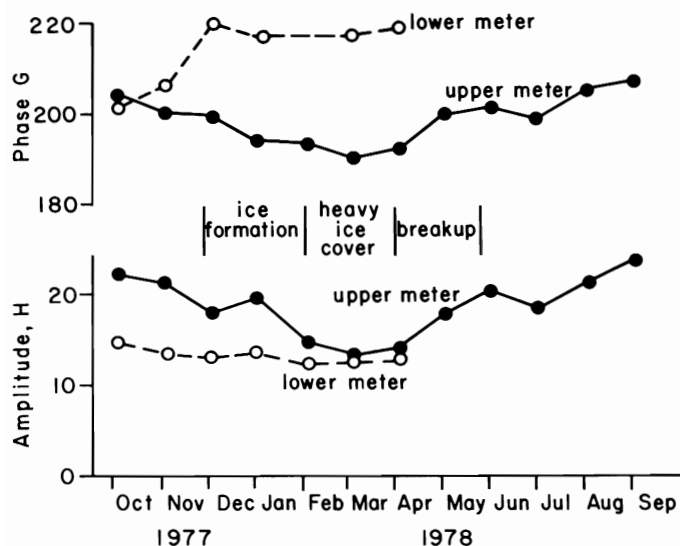


Figure 8-12. Variations in the  $M_2$  constituent of the east component of current at station NC24 for a one-year period beginning September 1977. Upper meter was at a depth of 24 m (19 m for the last two months). Lower meter depth was 40 m.

Phases at both meters also varied. At the upper meter phase decreased from  $204^\circ$  to  $190^\circ$  while at the lower meter phase increased from  $201^\circ$  to about  $217^\circ$ . This was associated with a shift in the ellipse axis orientation toward the left at the lower meter while the upper-meter ellipse remained steady. The  $K_1$  amplitudes were also reduced, although to a lesser extent than  $M_2$ . It is reasonably certain that these changes are associated with ice cover. Whether these phenomena were due more to a reduction of mooring noise resulting from wave attenuation by the ice or to frictional effects of ice cover remains unknown. Presumably, mooring noise would increase the amplitudes of all frequencies by more or less the same amount; moreover, phases would not be affected. Nevertheless, mooring noise is probably an important consideration, especially during the stormy fall and spring months.

The component harmonic constants for  $M_2$ ,  $N_2$ ,  $K_1$ , and  $O_1$  were converted to an ellipse representation to give amplitude  $H$  and phase  $G$  for the major axis, direction of the major axis, amplitude of the minor axis, and sense of rotation. Usually the analysis for the first 29 days of the mooring period was used, to minimize effects of fouling on the current harmonic constants. Table 8-1 gives the results of the analyses for a representative distribution of stations. Some stations were not included because of close proximity to one or more of those listed.

Plots of ellipses for stations listed are shown in Figs. 8-13 and 8-14 for the  $M_2$  and  $K_1$  constituents, respectively. Ellipses are centered at the station locations with lines from the center representing the constituent current vector for the time at which the equilibrium constituent passes the Greenwich meridian.

The  $M_2$  ellipses (Fig. 8-13) exhibit clockwise rotation at most stations south of St. Lawrence Island. The exception is BC14 near the Alaska Peninsula, which has nearly rectilinear motion. Axes are generally aligned in the direction of wave propagation, although topographic constraints can modify this, as at BC18, just south of Nunivak Island. Away from the influences of land, ellipses are more nearly circular. Amplitudes are typically 15-30 cm/sec on the open shelf, although somewhat higher speeds would be expected at the surface. In Norton Sound and near St. Lawrence Island, rotation is anticlockwise.  $M_2$  current speeds are small in Norton Sound.

The  $K_1$  ellipses (Fig. 8-14) are narrower than  $M_2$ . The orientation is aligned with flow in and out of the major embayments, Bristol Bay and Norton Sound. Over the outer shelf, the rotation is clockwise but becomes generally anticlockwise in the mid-shelf

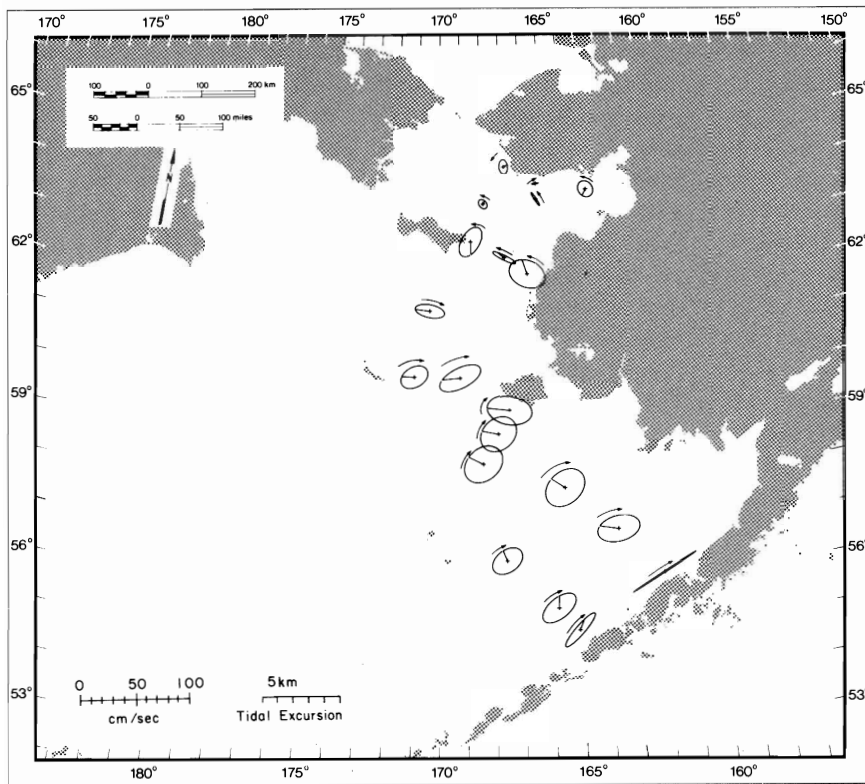


Figure 8-13.  $M_2$  current ellipses for stations listed in Table 8-2. For stations with records from two depths the ellipse for the deeper meter is plotted. Ellipses are centered on station location; line from center indicates constituent current vector when the  $M_2$  Greenwich equilibrium phase angle is  $0^\circ$ . Arrows indicate sense of rotation.

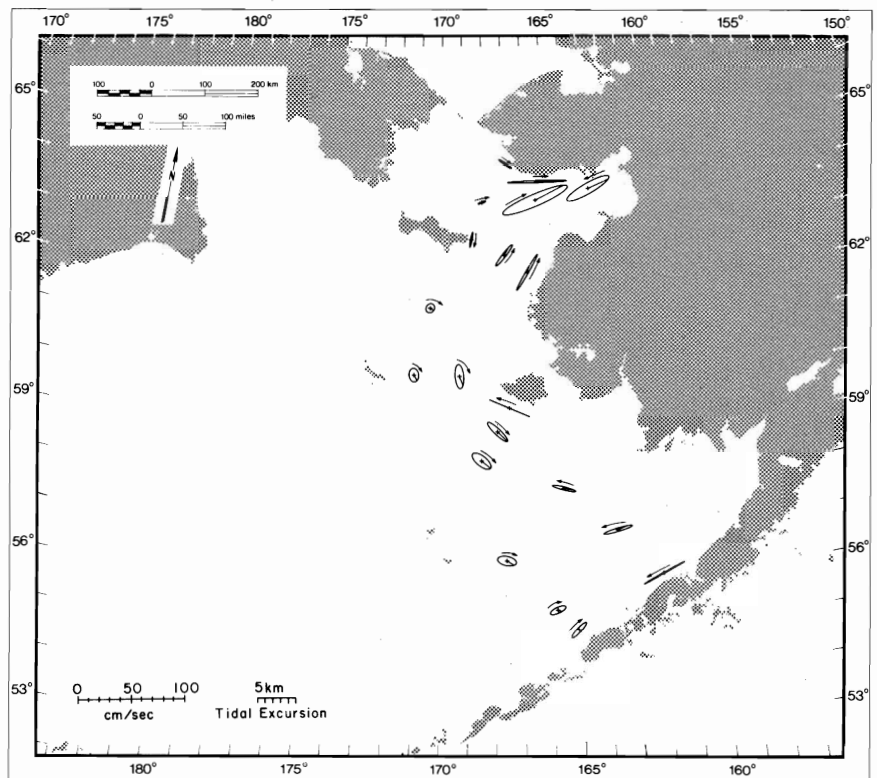


Figure 8-14. Same as 8-13 but for  $K_1$ .

TABLE 8-1

Results of 29-Day harmonic analyses for selected current-meter records, in ellipse representation<sup>1</sup>

Station	Depth	Meter	Depth	Lat N	Long W	O <sub>1</sub>			K <sub>1</sub>			N <sub>2</sub>			M <sub>2</sub>													
						major	min		major	min		major	min		major	min												
			Yr	JD	H	G	D	H	R	H	G	D	H	R	H	G	D	H	R									
BC3	114	20	55	02	165	10	76	150	7.9	245	52	1.7	C	9.8	279	57	1.0	C	6.5	26	37	1.8	C	26.4	71	38	7.6	C
BC3	114	100	55	02	165	10	76	150	7.8	265	52	1.2	C	10.4	281	48	2.1	C	4.9	11	50	0.6	C	21.0	61	47	4.4	C
BC13B	115	100	55	30	165	49	76	158	5.6	272	71	2.2	C	8.0	289	68	2.8	C	5.3	3	50	2.2	C	18.9	67	54	9.6	C
BC17	104	96	56	34	167	34	76	266	6.5	312	109	1.8	C	9.1	326	105	4.3	C	6.4	27	61	4.0	C	15.9	81	53	10.5	C
BC4	51	30	58	37	168	14	75	251	7.4	330	140	3.1	C	11.7	350	133	6.2	C	9.6	45	49	7.2	C	27.3	118	50	22.2	C
BC4	51	47	58	37	168	14	75	251	7.3	331	128	2.6	C	10.9	0	131	4.8	C	4.9	28	46	3.3	C	20.2	107	51	15.1	C
BC9	41	33	59	12	167	43	77	133	8.5	332	130	0.9	C	13.0	359	134	2.8	C	7.0	60	47	5.1	C	18.7	120	51	14.6	C
BC18	31	20	59	40	167	07	77	132	12.7	333	113	0.6	A	20.5	356	116	0.1	A	6.3	130	109	4.8	C	21.2	186	103	13.8	C
BC16	50	37	57	59	165	16	77	123	7.7	308	102	1.3	A	11.4	328	108	1.5	A	6.8	69	69	5.8	C	20.8	101	52	15.1	C
BC2	65	50	57	04	163	22	75	310	8.6	292	77	1.1	A	14.1	309	81	1.6	A	5.9	76	81	2.9	C	20.4	145	80	12.1	C
BC14	51	20	56	03	161	50	76	152	13.5	292	68	0.5	A	21.7	312	70	0.5	A	12.2	98	69	0.1	A	35.4	159	67	0.7	C
BC20	64	51	60	26	171	05	78	202	4.5	186	340	2.4	C	6.7	214	353	4.5	C	4.5	68	68	2.7	C	13.7	136	61	9.5	C
BC21	42	20	60	24	169	10	78	202	8.0	188	352	2.4	C	12.5	219	0	4.6	C	8.0	86	68	3.0	C	28.6	150	63	17.1	C
BC21	42	32	60	24	169	10	78	202	7.9	187	351	2.9	C	11.6	221	353	4.1	C	6.9	87	61	2.5	C	21.1	139	64	9.6	C
NC24	48	19	61	48	170	26	78	203	3.4	212	358	2.7	C	5.5	263	35	4.4	C	6.4	144	86	3.7	C	21.1	206	92	12.5	C
NC24	48	39	61	48	170	26	78	203	2.9	189	335	2.7	C	4.6	274	33	3.9	C	4.1	120	103	1.3	C	14.1	191	103	6.1	C
LD1	14	10	62	30	166	07	78	204	10.9	261	19	0.2	C	19.8	290	34	1.2	A	5.9	268	28	3.3	A	17.5	56	298	12.8	A
NC17	26	17	62	53	167	05	78	165	8.8	271	39	0.1	A	12.8	310	41	1.7	A	4.6	348	305	1.0	A	12.1	48	301	2.3	A
LD2	28	24	63	13	168	35	78	203	4.5	220	20	0.3	C	7.5	29	11	0.7	C	4.5	12	201	1.7	A	15.4	310	211	8.5	A
LD3	37	33	64	00	168	00	78	204	1.9	342	63	0.1	C	4.0	24	73	1.7	C	1.3	39	301	1.1	A	4.9	78	322	3.5	A
LD4	20	16	64	47	166	50	78	205	3.9	144	294	1.6	C	7.5	222	309	0.9	C	2.7	358	17	0.4	C	6.8	74	356	4.0	A
NC20	19	5	64	00	165	29	77	189	18.5	315	70	3.0	C	33.0	22	70	5.7	C	2.0	244	126	0.5	A	7.5	303	155	0.9	A
NC14	32	21	64	22	165	22	76	234	14.5	327	93	0.4	C	27.7	27	94	0.9	C	1.9	167	90	0.5	C	3.3	182	85	0.5	C
LD5	27	20	64	08	163	00	78	206	9.3	335	66	1.7	A	22.7	25	67	4.8	A	3.0	167	0	2.4	A	8.0	244	331	6.7	A

<sup>1</sup> Amplitudes H are cm/sec, phases G are referred to Greenwich, and direction D of major axis is compass degrees. C refers to clockwise rotation, A to anticlockwise. To obtain phase and direction of minor axis, add 90° to major axis phase if rotation is clockwise, or subtract 90° if anticlockwise.

region of Bristol Bay (stations BC16, BC2, BC14) and in the approaches to Norton Sound (stations LD1, LD2, NC17). Typical amplitudes over the southeast shelf are 10-20 cm/sec. Largest  $K_1$  currents are found within Norton Sound where amplitudes range from 20 to over 30 cm/sec. West of Norton Sound amplitudes are very small.

Ellipses for the smaller  $N_2$  and  $O_1$  constituents have not been plotted. Generally they are similar to the  $M_2$  and  $K_1$  respectively.  $O_1$  major axis amplitudes are 60-75 percent of  $K_1$  in the southeastern Bering Sea and 40-60 percent in the Norton Sound region.  $N_2$  is about 25-40 percent of  $M_2$  throughout the Bering Sea.

## DISCUSSION

Both models and observations show that the largest tides in the Bering Sea occur on the inner southeast Bering shelf. As shown in the figures, there is general agreement that the tides propagate as free waves onto the southeast shelf from the deep basin. In the vicinity of the Alaska Peninsula, the exponential decay of amplitude northward from shore and a comparison of the tidal heights and currents at BC14 indicate that the semidiurnal and diurnal tides are Kelvin<sup>2</sup> waves near the peninsula, the semidiurnal wave is progressive as at BC2, where the  $M_2$  phase difference is  $12^\circ$ , and at BC14, where the current is nearly in phase with the tide. Conversely, the  $K_1$  tide has a much larger standing wave component, with a phase difference of  $64^\circ$  at BC2 and about  $40^\circ$  at BC14. When the Kelvin waves propagate into the inner shelf, there is an interesting difference between the reflected waves for the two tidal species. The critical latitudes of the diurnal tides ( $\sim 30^\circ\text{N}$ ) lie south of the Bering Sea; diurnal tides can therefore obey only Kelvin-wave dynamics on the open shelf. The reflection of each diurnal tidal constituent produces a classic amphidromic system on the southeast shelf with the amphidromic point well offshore.

The critical latitudes of the semidiurnal tides ( $75^\circ\text{N}$  for  $M_2$ ) lie north of the Bering Sea. As a

<sup>2</sup> Kelvin and Sverdrup waves are long waves under the influence of the earth's rotation. In the northern hemisphere Kelvin waves propagate with the coast on the right and amplitude decreasing exponentially away from the coast. Current motion is rectilinear (in the absence of friction). Sverdrup waves (also called Poincaré or inertial-gravity waves) have horizontal wave crests and the currents form a clockwise-rotating ellipse. Sverdrup waves can exist only where the wave period is less than the inertial period. In areas where both Kelvin and Sverdrup waves can exist, the actual wave is some combination of the two. For further discussion, the reader is referred to a text such as *The Oceans* (Sverdrup et al. 1942).

result, semidiurnal tides can obey Sverdrup-wave as well as Kelvin-wave dynamics. The presence of a virtual amphidrome near Cape Newenham for each semidiurnal constituent suggests that a major portion (if not all) of the incident, semidiurnal Kelvin waves are dissipated or converted on reflection into Sverdrup waves. Perhaps the acute apex angle of Kvichak Bay, together with the presence of sharply protruding peninsulas, may produce an efficient conversion to semidiurnal Sverdrup waves. A large part of the semidiurnal tidal energy may also be dissipated over the extensive mud flats and shoals of the Kvichak and Nushagak Bays and Rivers. On the open shelf, the broad semidiurnal tidal ellipses have approximately  $45\text{-}50^\circ$  phases relative to the tidal heights in the direction of propagation. This fact and the fact that the offshore cophase lines are roughly parallel to the coast and widely separated indicate that the semidiurnal tides act as a standing Sverdrup (Poincaré) wave in this region due to cooscillation in Kuskokwim Bay. Further cooscillation is evident at BC11, just southwest of Nunivak Island, where the  $M_2$  tide actually leads that at stations farther seaward.

The *Coast Pilot*, published by the U.S. Department of Commerce (1964), notes that to the north of the southeast Bering shelf the currents in Etolin Strait between Nunivak Island and the mainland are sufficiently strong to prevent ice formation in winter. This may be due to tidal currents associated with the great differences in tidal phases between the north and south sides of Nunivak Island.

There is much less consensus about the tides in the north Bering Sea. The tides around St. Lawrence Island are particularly confusing. Harris (1904) shows the tide progressing from west to east along the south shore and then east to west along the north shore, so that all phases of the tide are found around the island. Leonov (1960) has branches of the tide progressing through the passes on the west and east sides of the island and meeting on the north side together with the tide from the Arctic Ocean; he discusses areas of convergence and divergence and abrupt changes in velocity as a result of the meeting of the tides of the Pacific and Arctic Oceans. Conversely, the Office of Climatology and Oceanographic Analysis Division (1961) chart shows very little effect on the tide from St. Lawrence Island with a fairly smooth progression of the tide northward across the shelf and through the Bering Strait. Coachman et al. (1975) inferred the presence of an amphidrome south of St. Lawrence Island from tidal differences of stations listed in the tide tables.

According to Sünderman's (1977) charts (Fig.

8-2), cophase lines converge on Southeast Cape, and there is probably cooscillation in the bight on the south side of the island with a reversal of phase progression. This may be responsible for the large phase differences noted by Coachman et al. (1975). The tide appears to progress through the pass between Northwest Cape and Siberia and thence west to east along the north shore of St. Lawrence Island to the vicinity of Northeast Cape, where it meets the wave progressing north along the Alaskan mainland. This results in nearly 180° phase difference between the  $M_2$  currents at LD1, near the Yukon Delta, and at LD2 near Northeast Cape. That is, current is northerly at LD1 when it is southerly at LD2. Station NC17, between these two stations, is in a transition zone; most motion is cross-channel.

Coachman et al. (1975) discussed measurements made at a current-meter mooring 90 km south of the Bering Strait. Tidal currents were mainly semidiurnal with amplitudes of 1-12 cm/sec and the current ellipse orientation was generally northeast-southwest to north-south. In the Bering Strait, Ratmanoff (1937) and Fleming and Heggarty (1966) did not find noticeable tidal currents while Bloom (1964) and Coachman and Aagaard (1966) found that tidal currents modulated the net northward flow.

Semidiurnal currents are especially small in Norton Sound south of Nome, for example at stations NC14 and NC20. These stations are in an antinode one-half wavelength from the head of the bay. Generally, semidiurnal tides and tidal currents are small throughout the Norton Sound and Bering Strait region, perhaps as a result of frictional dissipation across the broad Bering Sea shelf and Kelvin-wave dynamics (i.e., the Norton Sound amphidrome and small amplitudes to the west of a northward-progressing wave).

The diurnal tides appear to be simpler than the semidiurnal tides because they are restricted to Kelvin-wave dynamics and have longer wavelengths. Tidal height/tidal current phase relationships indicate predominantly standing-wave characteristics in southeast Bering Sea and Norton Sound although between St. Lawrence Island and the Alaskan mainland the tide is more progressive. Thus the diurnal tide in the deep western Bering Sea basin cooscillates with Bristol Bay and Norton Sound. Currents are highest in Norton Sound because of the shallower depth, even though the diurnal tides are higher at the head of Bristol Bay. Between St. Lawrence Island and the Bering Strait, the diurnal tides virtually disappear, again due to Kelvin-wave dynamics and dissipation.

While there is good agreement between the models and the observations on the major features of the

tides of the eastern Bering Sea shelf, there are some differences. For instance, the  $M_2$  cotidal chart of Sünderman (1977) has systematically higher amplitudes and later phases than the observations on the southeast shelf, but lower amplitudes in Kvichak Bay. Also, the actual amphidrome in Norton Sound appears to be further ashore. These differences may be due to the coarse grid (75 km) and high horizontal eddy viscosity ( $10^9$  cm<sup>2</sup>/sec) used in the model.

It is more difficult to evaluate the Liu and Leendertse (1978, 1979) model (Figs. 8-3-5) since many of the observations were used for boundary conditions and for tuning empirical parameters. The model and observations are therefore not independent. The cotidal charts (Fig. 8-4) present composite tides based on a Fourier analysis of 50 hours of computed data; therefore the cotidal charts represent sums of constituents within each species, with an arbitrary composite phase rather than one referred to Greenwich. For these reasons, no attempt will be made here to assess the accuracy of this model.

#### APPENDIX

Moorings usually consisted of one or two Aanderaa RCM-4 current meters on a taut wire, with the upper current meter at a depth of about 20 m, just below the subsurface float; the deeper one was below the pycnocline, about 10 m above the bottom. In the Norton Sound area, where depths are generally less than 30 m, moorings contained only one meter. The Aanderaa TG2 or TG3 pressure gauge, if present, either was placed in a well within the anchor or was attached to acoustic release, just above the anchor. Pressure-gauge resolution is claimed by the manufacturer to be better than 0.5 cm. Individual moorings were in place for periods of up to one year, with observations of some locations spanning as much as three years.

Data were processed by methods similar to those described in Charnell and Krancus (1976). No correction was made for atmospheric pressure in the pressure-gage data. In Aanderaa current meters, the recorded speed is an average over the data interval (15, 20, 30, 40, or 60 minutes) while direction is essentially instantaneous. To remove the phase difference between speed and direction, speeds at times  $T_n$  and  $T_{n+1}$  were averaged to give the speed corresponding to the direction at  $T_n$  before converting to east and north components of velocity. The data were low-pass filtered to remove noise (i.e., energy at frequencies  $>0.5$  cycle/hr) and resampled at hourly intervals. A second-order polynomial was then used to interpolate to even hours.

The Munk-Cartwright response method (Munk and Cartwright 1966) was used for tidal height analysis using procedures based on those suggested by Cartwright et al. (1969). The pressure record from Station BC20 was selected as a reference for all other stations because of its length (300 days) and location (near the center of the study area), and because the tide there is thought to be representative of that entering the shelf from the deep basin of the Bering Sea. The tide potential was used as a reference for the BC20 pressure record, using weights of 0,  $\pm 2$ , and  $\pm 4$  days for the diurnal and semidiurnal bands. For the other stations the reference series was a complex prediction based on the sixteen largest diurnal and semidiurnal harmonic constituents derived from the BC20 analysis using weights of 0,  $\pm 2$  days.

Results of high and low water analyses for many locations in the Bering Sea were obtained from the National Ocean Survey. High and low water analysis

gives the mean tide range and Greenwich high and low water lunitidal intervals HWI and LWI. According to Schureman (1958), if the tide is semidiurnal, the  $M_2$  amplitude can be estimated by multiplying the mean range by 0.47. The phase may be found by:

$$M_2^\circ = \frac{1}{2}(\text{HWI} + \text{LWI}) \times 28.984 + 90^\circ.$$

For current-meter data, a 29-day harmonic analysis based on Schureman (1958) was used. Constituents  $O_1$ ,  $K_1$ ,  $N_2$ ,  $M_2$ , and  $S_2$  are derived directly, and other constituents are inferred from these on the basis of equilibrium relationships. The harmonic method was used for currents because uncertainties in data quality and seasonal variations obviated the use of the slightly more accurate response method.

The results of these analyses are given in Table 8-1 (for current-meter data, the four major constituents in an ellipse representation) and in Table 8-2

TABLE 8-2

Results of response analyses for the new pressure-gage observations<sup>1</sup>

Station	Lat, N	Long, W	$O_1$		$P_1$		$K_1$		$N_2$		$M_2$		$S_2$		Start Date		Length Days			
			H	G	H	G	H	G	H	G	H	G	H	G	Yr	JD				
BC20	60	26	171	05	9.8	310	5.8	323	18.1	326	6.9	121	20.5	171	2.2	249	77	260	300	
BC3	55	01	165	10	26.4	304	13.3	317	40.9	319	15.8	40	41.9	89	3.2	2	76	077	73	
BC13B	55	30	165	49	23.8	311	11.4	322	34.4	325	13.2	52	35.5	106	1.8	327	76	158	114	
BC13D	55	47	165	23	23.0	312	11.0	324	33.4	327	15.0	56	39.0	109	1.4	314	77	252	131	
BC10	57	17	169	33	17.3	319	8.2	330	24.9	333	8.7	77	24.9	131	1.5	266	76	153	101	
BC4	58	37	168	14	6.3	305	3.9	300	12.4	303	11.1	98	33.4	151	1.8	252	75	250	58	
FX2	58	32	167	56	4.0	286	1.8	284	8.9	288	11.8	104	33.8	158	1.9	251	78	200	64	
BC9	59	13	167	42	2.4	220	3.1	253	9.7	258	12.4	108	36.7	164	2.0	246	76	269	230	
BC11	59	42	167	15	10.6	165	6.0	204	18.3	207	11.9	98	35.9	155	2.8	224	76	154	102	
BC21	60	23	169	11	7.4	271	5.3	294	16.6	297	10.1	136	30.9	189	2.9	265	77	260	246	
BC7	55	42	163	01	31.3	318	16.0	332	49.0	335	24.5	81	71.4	134	1.4	45	76	080	70	
BC2	57	04	163	22	19.0	358	9.3	11	28.3	13	14.7	102	45.2	157	0.5	343	76	151	200	
BC15	57	39	162	42	21.7	25	9.9	45	29.9	48	11.1	116	36.2	168	1.3	257	77	257	129	
LD1	62	30	166	07	17.9	286	10.3	319	31.7	324	13.2	274	46.1	328	6.8	49	78	204	54	
NC17	62	53	167	05	10.7	303	6.2	336	19.0	341	7.4	274	25.6	330	3.0	121	77	263	293	
NC18	63	09	168	23	4.4	339	2.9	351	8.9	356	4.7	272	22.4	324	2.6	59	76	245	120	
LD2	63	13	168	35	4.6	338	2.6	356	8.1	359	6.2	261	26.6	319	5.3	58	78	203	54	
LD4	64	47	166	50	2.3	75	1.1	218	4.2	222	2.3	47	4.9	138	0.6	324	78	205	55	
NC10	65	45	168	27	0.5	228	0.6	277	2.7	296	2.5	147	12.0	213	3.5	284	77	202	26	
GEO	64	00	165	30	9.5	23	4.8	66	14.0	71	4.4	349	13.0	44	2.5	131	77	189	60	
PROBE																				
LD5	64	08	163	00	16.9	60	10.4	106	32.1	110	1.0	186	2.0	233	0.2	277	78	206	41	
UN-ALAKLEET	65	53	160	47	24.0	55	13.9	102	42.9	108	5.2	164	17.3	222	3.0	326	77	220	95	

<sup>1</sup> Amplitude H in mbar of pressure. 1 mbar equals  $1.007 \pm 0.003$  cm of sea water in the Bering Sea. Phases G are referred to Greenwich.

(for pressure gauges, the six major constituents). Harmonic constant amplitudes  $H$  are cm/sec for currents and mbar for pressure-gauge data. For this region, 1 mbar equals  $1.007 \pm .003$  cm of sea water. Phases are referred to Greenwich.

#### ACKNOWLEDGMENTS

This chapter is contribution no. 431 from the NOAA/ERL Pacific Marine Environmental Laboratory. The work was supported in part by the Bureau of Land Management through interagency agreement with the National Oceanic and Atmospheric Administration, under which a multiyear program responding to needs of petroleum development of the Alaskan Continental Shelf is managed by the Outer Continental Shelf Environmental Assessment Program (OCSEAP) Office; and in part by NOAA's Environmental Research Laboratories.

The authors wish to express their appreciation to the following: L. Long and S. Wright of PMEL for data processing; B. Zetler of IGPP, S. K. Liu of Rand Corp., K. Aagaard and A. Clarke of the University of Washington, J. Schumacher, J. Larsen, and R. Preisendorfer of PMEL, T. Kinder of NORDA, and the anonymous reviewers for helpful suggestions; J. Fancher of the National Ocean Survey, D. Cacchione of the U. S. Geological Survey, and W. J. Ingraham, Jr. of the National Marine Fisheries Service for providing data; and J. Golly for drafting.



#### REFERENCES

- Bloom, G. L.  
1964 Water transport and temperature measurements in the eastern Bering Strait, 1953-1958. *J. Geophys. Res.* 69: 3335-54.
- Bogdanov, K. T.  
1961 New charts of the cotidal lines of semi-diurnal tidal waves ( $M_2$  and  $S_2$ ) for the Pacific Ocean. *Sov. Oceanog.* 1: 28-31.
- Bogdanov, K. T., K. V. Kim, and V. A. Magarik  
1964 Numerical solutions of tide hydrodynamic equations by means of BESM-2 electronic computer for the Pacific Area. *Trudy Inst. Okeanol. Akad. Nauk SSSR* 75: 73-98.
- Cartwright, D.  
1979 Tidal theory. *In: Symposium on long waves in the ocean*, Man. Rep. Series 53: 35-8. Marine Sciences Dir., Dep. of Fish. and Environ., Ottawa.
- Cartwright, D., W. Munk, and B. Zetler  
1969 Pelagic tidal measurements. *Trans. Amer. Geophys. Union* 50: 472-77.
- Charnell, R. L., and G. A. Krancus  
1976 A processing system for Aanderaa current meter data. NOAA Tech. Mem. ERL PMEL-6.
- Coachman, L. K., and K. Aagaard  
1966 On the water exchange through Bering Strait. *Limnol. and Oceanog.* 11: 44-59.
- Coachman, L. K., K. Aagaard, and R. B. Tripp  
1975 Bering Strait: The regional physical oceanography, Univ. of Washington Press, Seattle.
- Defant, A.  
1961 *Physical oceanography, II*, Pergamon Press, Oxford.
- Fleet Weather Facility  
1977-1978 Eastern-Western Arctic Sea ice analysis, Suitland, Md.
- Fleming, R. H., and D. Heggarty  
1966 Oceanography of the southeastern Chukchi Sea. *In: Environment of the Cape Thompson Region, Alaska.*, U. S. Atomic Energy Comm., Div. of Tech. Information, 697-754.
- Goodman, J. R., J. H. Lincoln, T. G. Thompson, and F. A. Zeusler  
1942 Physical and chemical investigations: Bering Sea, Bering Strait, Chukchi Sea during the summers of 1937 and 1938. Univ. of Washington Pub. Oceanog. 3. 105-69.

- Harris, J. R.  
 1904 Manual of tides, Part IV. Appendix 5. Rep. of Superintendent U. S. Coast and Geodetic Survey, Washington, D. C. 394-5.
- Hastings, J. R.  
 1976 A single-layer hydrodynamical-numerical model of the eastern Bering Sea shelf. *Mar. Sci. Comm.* 2: 335-56.
- International Hydrographic Bureau  
 1966 Tides, harmonic constants. Spec. Pub. No. 26, Monaco.
- Jeffreys, H.  
 1921 Tidal friction in shallow seas. *Phil. Trans. Roy. Soc. London, Ser. A*, 221: 237-64.
- Leendertse, J. J., and S. K. Liu  
 1977 A three-dimensional model for estuaries and coastal Seas: IV, Turbulent energy computation. The Rand Corp. R-2187-OWRT.
- Leonov, A. K.  
 1960 Regional oceanography, Part I, Leningrad. (transl.)
- Liu, S. K. and J. J. Leendertse  
 1978 Three-dimensional subgridscale-energy model of eastern Bering Sea. *Proc. XVI Coast. Eng., Conf. Amer. Soc. Civil Eng.*  
 1979 A three-dimensional model for estuaries and coastal seas: VI, Bristol Bay simulations. The Rand Corp. R-2405-NOAA.
- Mamayev, O. I.  
 1958 The influence of stratification on vertical turbulent mixing in the sea. *Izv. Geophys. Ser.:* 870-5.
- Munk, W. H., and D. Cartwright  
 1966 Tidal spectroscopy and prediction. *Phil. Trans. Roy. Soc. London, Ser. A.* 259: 533-81.
- Munk, W. H., and G. J. F. MacDonald  
 1960 The rotation of the Earth. Cambridge Univ. Press.
- Office of Climatology and Oceanographic Analysis Division  
 1961 Climatological and oceanographic atlas for mariners, 2, N. Pacific Ocean.
- Preisendorfer, R. W.  
 1979 A transport formulation of the tsunamic propagation problem. *Marine Geodesy* 2: 67-82.
- Ratmanoff, G. E.  
 1937 On water interexchange in Bering Strait. *Explorations of Seas of USSR.* Hydro. Pub. Leningrad and Moscow, 119-33. (transl.)
- Schureman, P.  
 1958 Manual of harmonic analysis and prediction of tides, Coast and Geodetic Survey, U. S. Dep. Comm. Washington, D. C.
- Sünderman, J.  
 1977 The semidiurnal principal lunar tide  $M_2$  in the Bering Sea. *Deutsche Hydrog. Zeitschrift* 30: 91-101.
- Sverdrup, H. U., M. W. Johnson, and R. H. Fleming  
 1942 The oceans. Prentice-Hall, Englewood Cliffs, N. J.
- United States Department of Commerce  
 1964 United States Coast Pilot 9: Pacific and Arctic coasts Alaska, Cape Spender to Beaufort Sea. U. S. Gov. Printing Office, Washington, D.C.

